

Linear and Nonlinear PT-symmetric Oligomers: A Dynamical Systems Analysis

M. Duanmu,¹ K. Li,¹ R.L. Horne,² P.G. Kevrekidis,¹ and N. Whitaker¹

¹*Department of Mathematics and Statistics, University of Massachusetts, Amherst MA 01003-4515, USA*

²*Department of Mathematics, Morehouse College, Atlanta, GA 30314**

In the present work we focus on the cases of two-site (dimer) and three-site (trimer) configurations, i.e. oligomers, respecting the parity-time (PT) symmetry, i.e., with a spatially odd gain-loss profile. We examine different types of solutions of such configurations with linear and nonlinear gain/loss profiles. Solutions beyond the linear PT-symmetry critical point as well as solutions with asymmetric linearization eigenvalues are found in both the nonlinear dimer and trimer. The latter feature is absent in linear PT-symmetric trimers, while both of them are absent in linear PT-symmetric dimers. Furthermore, nonlinear gain/loss terms enable the existence of both symmetric and asymmetric solution profiles (and of bifurcations between them), while only symmetric solutions are present in the linear PT-symmetric dimers and trimers. The linear stability analysis around the obtained solutions is discussed and their dynamical evolution is explored by means of direct numerical simulations. Finally, a brief discussion is also given of recent progress in the context of PT-symmetric quadrimers.

I. INTRODUCTION

In the late 1990s, a radical yet well physically motivated proposal emerged in the context of the study of fundamentals of quantum mechanics. This was the suggestion of Bender and co-workers [1] that Hamiltonians that respect two principal physical symmetries of the dynamics, namely Parity (P) and Time-reversal (T) could enable the identification of real eigenvalues, which is a property which is highly desirable for operators associated with measurable quantities, even if the associated Hamiltonians are not Hermitian. A caveat in that regard, however, was that as the gain/loss parameter introduced in these non-Hermitian Hamiltonians was varied, a transition was quantified and termed the PT-symmetry breaking transition, beyond which the eigenvalues of the relevant operator were no longer purely real. It is interesting to note here that a prototypical playground where such ideas can be explored is that of standard Schrödinger Hamiltonians of the form $H = -(1/2)\Delta + V(x)$, for which in the case of a complex potential V , it is straightforward to see that the above constraints of PT symmetry amount to the potential satisfying the condition $V(x) = V^*(-x)$.

While the initial proposal of the above possibility was one of mathematical origin (rather than one inspired by a specific physical application), in the past few years, a significant vein of potential applications of such Hamiltonians has been initiated, predominantly so in the field of nonlinear optics. There, the work of Christodoulides and co-workers [2] gave rise to the realization that the synthetic systems that can be engineered therein enable a potential balance of gain (through suitable amplifiers) and the abundantly present losses in order to produce experimental realizations of PT-symmetric systems. An additional feature present in such settings which made both their theoretical and experimental investigation even more interesting was the presence of nonlinearity which, in turn, rendered worthwhile the exploration of the dynamics of nonlinear waves (such as bright or gap solitons [2] and more recently of dark solitons and vortices [3]). The above optical settings were in fact the ones that enabled the first experimental realizations of PT-symmetry. This was done in the context of waveguide couplers (i.e., either two waveguides with and without loss [4] – the so-called passive PT– or in the more “standard” case of one waveguide with gain and one with loss [5]). More recently, electronic analogs of such systems have been engineered in the work of [6]. In parallel to these pioneering steps in the realm of experiments, numerous theoretical investigations have arisen both in the context of linear PT-symmetric potentials [7–23] and even in the case of the so-called nonlinear PT-symmetric potentials (whereby a PT-symmetric type of gain/loss pattern appears in the nonlinear term) [24–26].

In the present work, we revisit this theme of both linear and nonlinear PT-symmetric potentials. We do so in the special context of the recently proposed PT-symmetric “oligomers”, namely few site configurations, which are not necessarily couplers (i.e., dimers) but rather can also be trimers, quadrimers etc. For the sake of illustration, we restrict ourselves to dimers and trimers herein but briefly also touch upon recent works in the context of quadrimers. In what follows below, we study the case of nonlinear-PT-symmetric dimers [24] and trimers and subsequently restrict considerations to the case of their linear-PT-symmetric analogs [13]. One of the fundamental side-effects of the fact

*Electronic address: rhorne@morehouse.edu

that the nonlinearity does *not* commute with the PT operator is the existence of nonlinear solutions that persist past the linear PT-phase-transition threshold. Furthermore, one of the principal consequences of the presence of gain/loss terms in the nonlinearity is the existence of both symmetric and asymmetric (in their amplitude) stationary solutions, with the latter possessing a non-symmetric linearization spectrum. Interesting bifurcation phenomena (such as spontaneous symmetry breakings) are, additionally, found to arise in this case. Our presentation is structured as follows: we first examine the nonlinear-PT-symmetric dimer in section II (existence of solutions in II.A, linear stability setup in II.B and numerical results in II.C), while the corresponding analysis for the trimer is done in section III. In section IV, we review the corresponding case of linear-PT-symmetric oligomers, while in section V, we summarize our findings and present our conclusions.

II. ANALYSIS OF STATIONARY SOLUTIONS FOR THE NONLINEAR-PT-SYMMETRIC DIMER CASE

We first consider the so-called PT-symmetric coupler or dimer, in which a gain/loss pattern appears *both* in the linear and nonlinear terms. The dynamical equations have the form:

$$\begin{aligned} iu_t &= -\epsilon v + (\rho_r - i\rho_{im})|u|^2 u + i\gamma u \\ iv_t &= -\epsilon u + (\rho_r + i\rho_{im})|v|^2 v - i\gamma v. \end{aligned} \quad (1)$$

The model contains the Kerr nonlinearity which is relevant to optical waveguides and is effectively a generalization of the experimental framework of [5], in that nonlinear (i.e., amplitude-dependent) gain and loss processes are taken into account. We have used $u(t)$ and $v(t)$ to denote the two complex-valued variables for the dimer and the evolution variable is t (in optics, this is actually a spatial variable standing for the propagation distance along the optical crystal). Considering the prototypical stationary solutions of the system, we let $u(t)$ and $v(t)$ have the forms:

$$u(t) = ae^{iEt}, \quad v(t) = be^{iEt} \quad (2)$$

where E is the propagation constant while the complex numbers a and b denote the amplitudes of the dimer sites. Plugging this ansatz into Eq. (1), one finds the complex nonlinear algebraic equations:

$$\begin{aligned} Ea &= \epsilon b - (\rho_r - i\rho_{im})|a|^2 a - i\gamma a \\ Eb &= \epsilon a - (\rho_r + i\rho_{im})|b|^2 b + i\gamma b. \end{aligned} \quad (3)$$

We now use a polar decomposition of a and b of the form:

$$a = Ae^{i\phi_a}, \quad b = Be^{i\phi_b} \quad (4)$$

for real-valued A , B , ϕ_a and ϕ_b . Plugging Eq. (4) into Eq. (3) and writing these equations in terms of their real and imaginary parts, we find:

$$\begin{aligned} EA &= \epsilon B \cos(\phi_b - \phi_a) - \rho_r A^3 \\ EB &= \epsilon A \cos(\phi_b - \phi_a) - \rho_r B^3 \\ -\epsilon A \sin(\phi_b - \phi_a) - \rho_{im} B^3 + \gamma B &= 0 \\ \epsilon B \sin(\phi_b - \phi_a) + \rho_{im} A^3 - \gamma A &= 0. \end{aligned} \quad (5)$$

The last two equations yield

$$(A^2 - B^2) [\rho_{im}(A^2 + B^2) - \gamma] = 0. \quad (6)$$

We note that Eq. (6) yields a simple algebraic condition which connects the amplitude of the two dimer sites. This allows us to distinguish several subcases of interest. We look for nontrivial solutions A and B in each of the subcases presented in the following section.

A. Existence of Localized Modes for the Dimer Case

Eq. (6) identifies the different scenarios for the values of A and B . We now examine the three cases that arise from this equation for our dimer dynamical system.

- Case I : $A^2 = B^2$ and $A^2 + B^2 \neq \gamma/\rho_{im}$:

Recall the equations given in (5):

$$EA = \epsilon B \cos(\phi_b - \phi_a) - \rho_r A^3; \quad EB = \epsilon A \cos(\phi_b - \phi_a) - \rho_r B^3 \quad (7)$$

and

$$\epsilon B \sin(\phi_b - \phi_a) + \rho_{im} A^3 - \gamma A = 0; \quad -\epsilon A \sin(\phi_b - \phi_a) - \rho_{im} B^3 + \gamma B = 0. \quad (8)$$

Since $A = B$ (i.e., these are symmetric solutions) in this case, the two equations in each set are equivalent. Thus, we have:

$$\sin(\phi_b - \phi_a) = \frac{-(\rho_{im} A^2 - \gamma)}{\epsilon}, \quad \cos(\phi_b - \phi_a) = \frac{\rho_r A^2 + E}{\epsilon}. \quad (9)$$

We use the relation $\sin^2(\phi_b - \phi_a) + \cos^2(\phi_b - \phi_a) = 1$ to determine the following quadratic equation for A^2 :

$$(\rho_r^2 + \rho_{im}^2)A^4 + 2(E\rho_r - \gamma\rho_{im})A^2 + \gamma^2 + E^2 - \epsilon^2 = 0. \quad (10)$$

The solution of the resulting bi-quadratic equation reads:

$$A^2 = B^2 = \frac{-(E\rho_r - \gamma\rho_{im}) \pm \sqrt{(E\rho_r - \gamma\rho_{im})^2 - (\rho_r^2 + \rho_{im}^2)(\gamma^2 + E^2 - \epsilon^2)}}{\rho_r^2 + \rho_{im}^2}, \quad (11)$$

with the restriction that

$$(E\rho_r - \gamma\rho_{im})^2 \geq (\rho_r^2 + \rho_{im}^2)(\gamma^2 + E^2 - \epsilon^2). \quad (12)$$

- Case II : $A^2 + B^2 = \gamma/\rho_{im}$ and $A^2 \neq B^2$:

Under these conditions, one can get

$$A^2 = \frac{\gamma}{2\rho_{im}} \pm \sqrt{\frac{\gamma^2}{4\rho_{im}^2} - \frac{\epsilon^2}{\rho_r^2 + \rho_{im}^2}} \quad (13)$$

$$B^2 = \frac{\gamma}{2\rho_{im}} \mp \sqrt{\frac{\gamma^2}{4\rho_{im}^2} - \frac{\epsilon^2}{\rho_r^2 + \rho_{im}^2}} \quad (14)$$

$$E = -\frac{\gamma\rho_r}{\rho_{im}} \quad (15)$$

$$\cos(\phi_b - \phi_a) = -\frac{\epsilon\rho_r}{\sqrt{\rho_r^2 + \rho_{im}^2}}, \quad (16)$$

with the restriction that

$$\frac{\gamma^2}{4\rho_{im}^2} \geq \frac{\epsilon^2}{\rho_r^2 + \rho_{im}^2}. \quad (17)$$

A fundamental difference of this case from case I is that here E is no longer a free parameter [24]. The solutions with the different amplitudes will be called asymmetric in what follows.

- Case III : $A^2 + B^2 = \gamma/\rho_{im}$ and $A^2 = B^2$:

As a final “mixed” possibility, between the above symmetric and asymmetric cases, from Eq. (5), it is straightforward to obtain

$$A = B = \sqrt{\frac{\gamma}{2\rho_{im}}}, \quad (18)$$

$$\cos(\phi_b - \phi_a) = \frac{2\rho_{im}E + \gamma\rho_r}{2\epsilon\rho_{im}} \quad (19)$$

$$\sin(\phi_b - \phi_a) = \frac{\gamma}{2\epsilon}, \quad (20)$$

with the restriction that

$$\left(\frac{2\rho_{im}E + \gamma\rho_r}{2\epsilon\rho_{im}}\right)^2 + \left(\frac{\gamma}{2\epsilon}\right)^2 = 1. \quad (21)$$

Once again this implies that once other parameters (such as γ , ρ_{im} , ρ_r and ϵ are determined, E is not a free parameter but rather is obtained from Eq. (21). These will be referred to as special symmetric solutions in the following.

It is particularly important to highlight that both solutions of Case II (asymmetric) and ones of Case III (special symmetric) are present due to competing effects of the linear and nonlinear gain loss profiles; notice the opposite signs thereof in Eq. (1) and the necessity of $\gamma\rho_{im} > 0$ for such solutions to exist. In the case, where the linear and nonlinear gain/loss cooperate (rather than compete) such solutions would obviously be absent and the system would be inherently less wealthy in its potential dynamics. This point was also discussed in [24].

B. Linear Stability Analysis for the Dimer Case

We now go back to our original PT-symmetric dimer with linear and nonlinear gain and loss in Eq. (1) and examine the linear stability of the solutions to this equation. We begin by setting

$$u(t) = e^{iEt}[a + pe^{\lambda t} + Pe^{\lambda^*t}], \quad v(t) = e^{iEt}[b + qe^{\lambda t} + Qe^{\lambda^*t}] \quad (22)$$

where λ is a complex-valued eigenvalue parameter revealing the growth (instability) or oscillation (stability) of all the modes of linearization of the dimer system; * denotes the complex conjugate and p, P, q, Q are perturbations to the solutions of interest. Plugging Eq. (22) into Eq. (1) and taking only the linear terms in p, P, q and Q , we find the following eigenvalue problem:

$$\mathbf{A}\mathbf{X} = i\lambda\mathbf{X} \quad (23)$$

where $\mathbf{X} = (p, -P^*, q, -Q^*)^T$ and \mathbf{A} is written as:

$$\mathbf{A} = \begin{pmatrix} a_{11} & -a^2(\rho_r - i\rho_{im}) & -\epsilon & 0 \\ (a^*)^2(\rho_r + i\rho_{im}) & a_{22} & 0 & \epsilon \\ -\epsilon & 0 & a_{33} & -b^2(\rho_r + i\rho_{im}) \\ 0 & \epsilon & (b^*)^2(\rho_r - i\rho_{im}) & a_{44} \end{pmatrix} \quad (24)$$

where

$$\begin{aligned} a_{11} &= E + 2|a|^2(\rho_r - i\rho_{im}) + i\gamma \\ a_{22} &= -2|a|^2(\rho_r + i\rho_{im}) - E + i\gamma \\ a_{33} &= E - i\gamma + 2|b|^2(\rho_r + i\rho_{im}) \\ a_{44} &= -E - i\gamma - 2|b|^2(\rho_r - i\rho_{im}). \end{aligned} \quad (25)$$

The use of the symmetric, asymmetric or mixed solutions of the previous subsection into these matrix elements produces a 4×4 complex matrix whose eigenvalues will determine the spectral stability of the corresponding nonlinear solution. The existence of eigenvalues with positive real part $\lambda_r > 0$ amounts to a dynamical instability of the relevant solution, while in the case where all 4 eigenvalues have $\lambda_r \leq 0$, the solution is linearly stable.

C. Numerical Results for the Dimer Case

Fig. 1 shows the profile of the different branches for the dimer case and for parameters $\epsilon = 1$, $E = 1$, $\rho_r = -2$ and $\rho_{im} = 1$ (unless noted otherwise). The branches denoted by blue stars and red diamonds correspond to the case I of symmetric solutions; these two branches collide and disappear at the critical point $\gamma = 1.61$ (when Eq. (12) becomes an equality). The green circle and magenta cross branches correspond to case II; and the black squares branch corresponds to case III. For the latter two branches, when γ is varied, E is also varied too (rather than staying fixed at $E = 1$ as for case I) according to Eqs. (15) and (21), respectively. Similar notations are used in Fig. 2, which shows the linear stability eigenvalues $\lambda = \lambda_r + i\lambda_i$ of the linearization. While the branches of case I are stable, it is interesting to note that the branch of case III (black squares) is stable until a pitchfork (symmetry breaking) bifurcation arises at $\gamma = 0.895$ (when Eq. (17) becomes an equality) and acquires a real pair of eigenvalues thereafter signalling its dynamical instability. On the other hand, it is at that critical point that the two branches belonging to case II arise. While the special symmetric black squares' branch of case III persists up to the critical point of $\gamma = 2\epsilon = 2$ of Eq. (20), it should be pointed out that nonlinearity enables the asymmetric branches of Case II to persist for large values of γ , in fact well past the point of the linear PT phase transition. This feature has been highlighted in a number of recent works [13, 27]; in the case of the dimer the linear critical PT phase transition point is identified as $\gamma = \epsilon$, while for the trimer setting considered below it is $\gamma = \sqrt{2}\epsilon$.

An additional point worthy to mention here is that in linear PT-symmetric chains (just as is the case in typical Hamiltonian systems), if λ is an eigenvalue to the linearization problem around a solution, so are $-\lambda$, $\bar{\lambda}$, and $-\bar{\lambda}$ (where the overbar denotes complex conjugation here). However, in our nonlinear PT-symmetric dimer $-\lambda$ and $-\bar{\lambda}$ may not appear in the linearization around a particular branch, as is observed in Fig. 2. Eigenvalues of the green circles and magenta cross branches are not symmetric about the imaginary axis, but are symmetric with respect to each other. One can see from Fig. 3 that the green circles branch is always stable, while the magenta crosses branch is always unstable (due to an oscillatory instability associated with a complex eigenvalue pair). This is because the existence of asymmetry in these solutions of case II creates, in turn, asymmetries in the linearization matrix, due to the nonlinear gain/loss term, which breaks the PT symmetry of the linearization matrix and produces the corresponding observable asymmetry in eigenvalues.

The dynamical evolution of the different elements of the bifurcation diagram of nonlinear-PT-symmetric dimer is shown in Fig. 3 at a fixed $\gamma = 1.5$. In all the cases here and below, where a stationary solution exists for the parameter value for which it is initialized, a numerically exact solution up to 10^{-8} is typically used as an initial condition in the system. The system is sufficiently sensitive to dynamical instabilities that even the amplification of roundoff errors are enough to observe them. The stability of the case I branches is evident in the invariance of the relevant states during the course of the simulation (blue stars and red diamonds). On the other hand, the black squares branch is attracted towards the asymmetric (yet stable, as is evident in the corresponding simulation) green circles branch. Finally, the asymmetric magenta crosses branch leads to indefinite growth of the site with the larger amplitude (nonlinear gain) and the decay of the site with the smaller amplitude (nonlinear loss).

III. ANALYSIS OF STATIONARY SOLUTIONS FOR THE NONLINEAR-PT-SYMMETRIC TRIMER CASE

We now consider the generalization of the above considerations to the case of a so-called PT-symmetric trimer. Here, the dynamical system associated with a potential application of a three-waveguide setting is of the form:

$$\begin{aligned} iu_t &= -\epsilon v + (\rho_r - i\rho_{im})|u|^2 u + i\gamma u \\ iv_t &= -\epsilon(u + w) - |v|^2 v \\ iw_t &= -\epsilon v + (\rho_r + i\rho_{im})|w|^2 w - i\gamma w \end{aligned} \tag{26}$$

Such configurations have been considered earlier in optical applications theoretically [28] and even experimentally [29] in the absence of gain/loss. Here in the spirit, of [5] (and also of [13]), we examine this case with both linear and nonlinear gain/loss profiles. Once again, as in the case of the dimer, we present the richer phenomenology setting of direct competition between linear and nonlinear gain/loss. The middle site is assumed as devoid of gain and loss. The Kerr nonlinearity is also assumed to be present in all three sites. Here, we use $u(t)$, $v(t)$ and $w(t)$ as the complex-valued components for the trimer. For the stationary solutions, we again assume:

$$u(t) = ae^{iEt}, \quad v(t) = be^{iEt} \quad \text{and} \quad w(t) = ce^{iEt}. \tag{27}$$

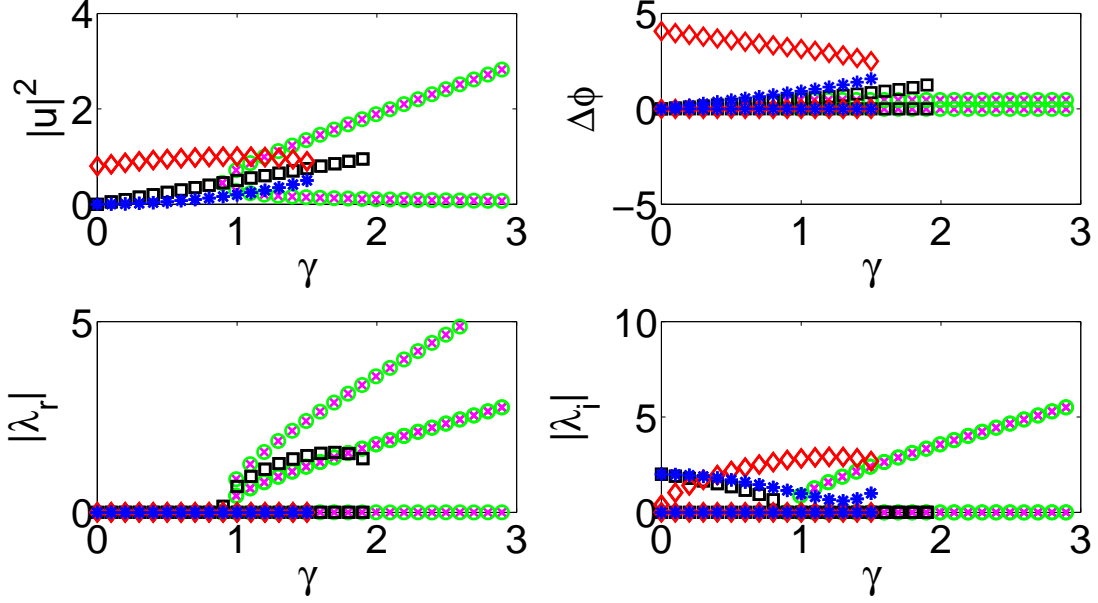


FIG. 1: The solution profiles of the nonlinear PT-symmetric dimer case with $\epsilon = 1$, $\rho_r = -2$ and $\rho_{im} = 1$. The four panels here present the continuation of each branch (the amplitudes in the top left, the phases in the top right, and the real -bottom left- and imaginary -bottom right- parts of the linear stability eigenvalues) starting from the conservative system at $\gamma = 0$. The five branches are denoted by curves of blue stars, red diamonds, black squares, green circles and magenta crosses. Blue stars: Case I with “-” in the amplitude; Red diamonds: Case I with “+” in the amplitude; Green circles: Case II with “+” in the amplitude (of A); Magenta crosses: Case II with “-” in the amplitude (of A); Black squares: Case III. Notice that the eigenvalues of green circles and magenta crosses are opposite to each other (see the relevant discussion in the text). We always set $E = 1$ in the case I branches, namely the blue stars and the red diamonds, which terminate at the same point when $\gamma = 1.61$. The black squares are subject to a destabilizing supercritical pitchfork bifurcation at $\gamma = 0.895$, $E = 1.789$ whereby the green circles and magenta crosses arise. The black squares branch terminates at $\gamma = 2$; the green circles and magenta crosses exist for arbitrary values of the (linear) gain/loss past the linear PT-symmetry breaking point.

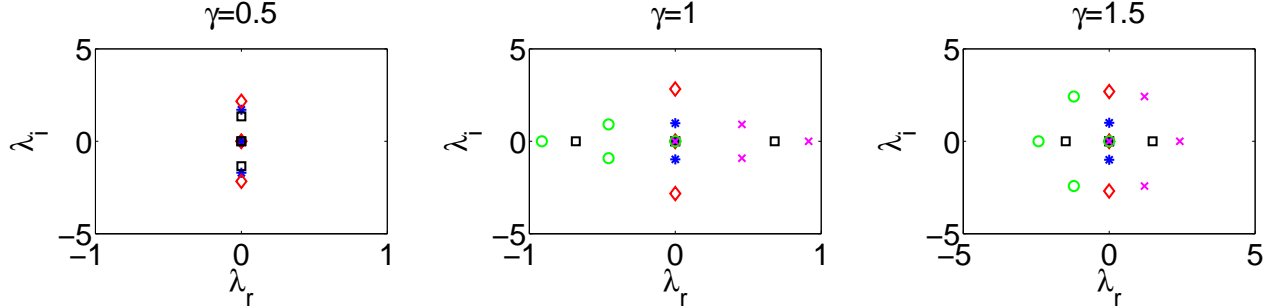


FIG. 2: The eigenvalue plots illustrating the linear stability of the nonlinear-PT-symmetric dimer with $\epsilon = 1$, $\rho_r = -2$ and $\rho_{im} = 1$. For the blues stars and red diamonds branches, we use $E = 1$ here, while for the case II (green circles and magenta crosses) and case III (black squares), E is determined from the remaining parameters based on Eqs. (15) and (21), respectively.

Plugging Eqs. (27) into Eq. (26), we find:

$$Ea = \epsilon b - (\rho_r - i\rho_{im})|a|^2 a - i\gamma a, \quad Eb = \epsilon(a + c) + |b|^2 b$$

$$Ec = \epsilon b - (\rho_r + i\rho_{im})|c|^2 c + i\gamma c. \quad (28)$$

Since a, b and c are complex-valued functions, we use the polar decomposition:

$$a = Ae^{i\phi_a}, \quad b = Be^{i\phi_b} \quad \text{and} \quad c = Ce^{i\phi_c} \quad (29)$$

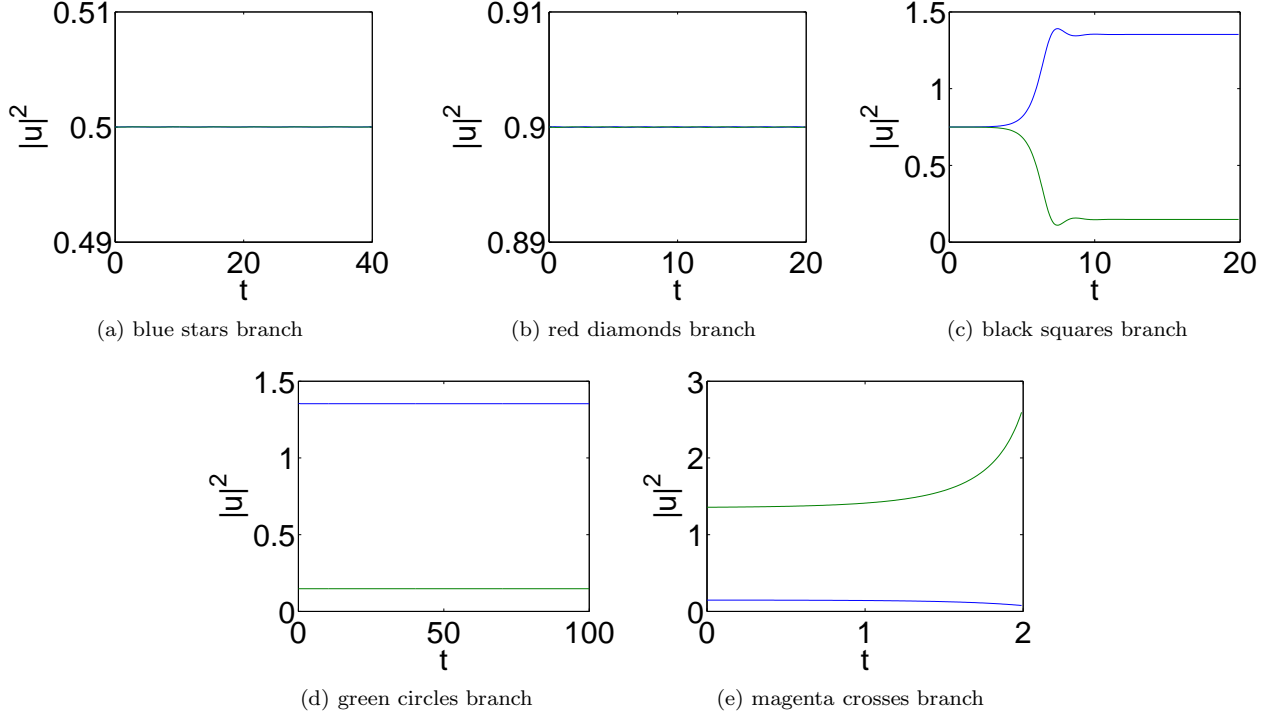


FIG. 3: The dynamical evolution plots of the branches for the case of the nonlinear-PT-symmetric dimer with the same parameter settings as in Fig. 2 when $\gamma = 1.5$. The symmetric blue stars and red diamonds of Case I and the asymmetric green circles of Case II are stable, while the black squares of Case III (past the pitchfork point) and magenta crosses of Case II are unstable and deviate from their initial profile during the dynamics (see also the discussion in the text).

where A, B, C, ϕ_a, ϕ_b and ϕ_c are real-valued. Plugging Eq. (29) into Eq. (28) and separating the real and imaginary parts, we derive the following set of real-valued equations for A, B and C :

$$\begin{aligned}
 EA &= \epsilon B \cos(\phi_b - \phi_a) - \rho_r A^3, & \epsilon B \sin(\phi_b - \phi_a) + \rho_{im} A^3 - \gamma A &= 0 \\
 EB &= \epsilon A \cos(\phi_b - \phi_a) + \epsilon C \cos(\phi_b - \phi_c) + B^3, & -\epsilon A \sin(\phi_b - \phi_a) - \epsilon C \sin(\phi_b - \phi_c) &= 0 \\
 EC &= \epsilon B \cos(\phi_b - \phi_c) - \rho_r C^3, & \epsilon B \sin(\phi_b - \phi_c) - \rho_{im} C^3 + \gamma C &= 0.
 \end{aligned} \tag{30}$$

We seek nontrivial solutions to Eqs. (30), i.e., $(A, B, C) \neq (0, 0, 0)$. We can reduce Eqs. (30) to the form:

$$\begin{aligned}
 \cos(\phi_b - \phi_a) &= \frac{EA + \rho_r A^3}{\epsilon B}, & \cos(\phi_b - \phi_c) &= \frac{EC + \rho_r C^3}{\epsilon B} \\
 \sin(\phi_b - \phi_a) &= \frac{\gamma A - \rho_{im} A^3}{\epsilon B}, & \sin(\phi_b - \phi_c) &= -\frac{(\gamma C - \rho_{im} C^3)}{\epsilon B} \\
 A \cos(\phi_b - \phi_a) + C \cos(\phi_b - \phi_c) &= \frac{EB - B^3}{\epsilon}, & A \sin(\phi_b - \phi_a) + C \sin(\phi_b - \phi_c) &= 0.
 \end{aligned} \tag{31}$$

We apply the first four equations of Eqs. (31) into the last two equations and obtain the following relations:

$$B^4 - EB^2 + E(A^2 + C^2) + \rho_r(A^4 + C^4) = 0, \quad (A^2 - C^2)[\gamma - \rho_{im}(A^2 + C^2)] = 0. \tag{32}$$

We now determine A, B and C for several subcases (symmetric, asymmetric and mixed) as was done for the dimer case in section II.

A. Existence of Localized Modes for the Trimer Case

For the trimer case, the special cases that can be seen to emerge for the solutions of Eqs. (32) can be classified as follows:

- Case I : $A^2 = C^2$ and $A^2 + C^2 \neq \gamma/\rho_{im}$:

In this case the algebraic equations assume the form:

$$\begin{aligned}\cos(\phi_b - \phi_a) &= \frac{EA + \rho_r A^3}{\epsilon B} = \cos(\phi_b - \phi_c) \\ \sin(\phi_b - \phi_a) &= \frac{\gamma A - \rho_{im} A^3}{\epsilon B} = -\sin(\phi_b - \phi_c).\end{aligned}\quad (33)$$

We now use Eq. (32) and $\cos^2(\phi_b - \phi_a) + \sin^2(\phi_b - \phi_a) = 1$ to determine:

$$(\rho_r^2 + \rho_{im}^2)A^6 + 2(E\rho_r - \gamma\rho_{im})A^4 + (E^2 + \gamma^2)A^2 - \epsilon^2 B^2 = 0, \quad B^4 - EB^2 + 2EA^2 + 2\rho_r A^4 = 0. \quad (34)$$

One can solve eqns. (34) for A^2 and B^2 to complete the calculation of the relevant symmetric branch of solutions of Case I.

- Case II : $A^2 + C^2 = \gamma/\rho_{im}$ and $A^2 \neq C^2$:

From Eq. (31), we obtain the four algebraic equations:

$$\begin{aligned}A^2(E + \rho_\gamma A^2)^2 + A^2(\gamma - \rho_{im} A^2)^2 &= \epsilon^2 B^2 \\ C^2(E + \rho_\gamma C^2)^2 + C^2(\gamma - \rho_{im} C^2)^2 &= \epsilon^2 B^2 \\ A^2 + C^2 &= \frac{\gamma}{\rho_{im}} \\ B^4 - EB^2 + E(A^2 + C^2) + \rho_r(A^4 + C^4) &= 0.\end{aligned}\quad (35)$$

We now have four equations but with only three unknowns (A , B and C). Therefore, in contrast to the previous symmetric branch of case I, one of the parameters E , ϵ , ρ_r , ρ_{im} , γ is determined by the other four; i.e., not all four of these parameters can be picked independently in order to give rise to a solution of the trimer. Once again, we should nevertheless, highlight here that these asymmetric solutions only exist because of the interplay of linear gain/loss and nonlinear loss/gain profiles.

- Case III : $A^2 + C^2 = \gamma/\rho_{im}$ and $A^2 = C^2$:

In this mixed case, we have

$$\begin{aligned}A^2 = C^2 &= \frac{\gamma}{2\rho_{im}} \\ B^4 - EB^2 + 2EA^2 + 2\rho_r A^4 &= 0,\end{aligned}\quad (36)$$

with the restriction that

$$E^2 - \frac{4E\gamma}{\rho_{im}} - \frac{2\rho_r\gamma^2}{\rho_{im}^2} \geq 0. \quad (37)$$

One can solve the following equations for B and E

$$\begin{aligned}B^4 - EB^2 + 2E\frac{\gamma}{2\rho_{im}} + 2\rho_r\frac{\gamma^2}{4\rho_{im}^2} &= 0 \\ (\rho_\gamma^2 + \rho_{im}^2)\frac{\gamma^3}{8\rho_{im}^3} + (2\rho_{im}E - 2\rho_{im}\gamma)\frac{\gamma^2}{4\rho_{im}^2} + (E^2 + \gamma^2)\frac{\gamma}{2\rho_{im}} &= \epsilon^2 B^2.\end{aligned}\quad (38)$$

These equations imply that one of the parameters (e.g., E) will be determined once the parameters, γ , ϵ , ρ_r and ρ_{im} are chosen.

B. Linear Stability Analysis for the Trimer Case

We again consider the nonlinear PT-symmetric trimer model with linear and nonlinear gain/loss and examine the linear stability of its solutions given in Eq. (26) for the solutions given in the previous section. We begin by positing the linearization ansatz:

$$\begin{aligned} u(t) &= e^{iEt}[a + pe^{\lambda t} + Pe^{\lambda^* t}], & v(t) &= e^{iEt}[b + qe^{\lambda t} + Qe^{\lambda^* t}] \\ w(t) &= e^{iEt}[c + re^{\lambda t} + Re^{\lambda^* t}] \end{aligned} \quad (39)$$

where p, P, q, Q, r, R are perturbations to the solutions of interest. Plugging Eq. (39) into Eq. (26) and truncating at the linear order in p, P, q, Q, r and R , we derive the following eigenvalue problem:

$$\mathbf{A}\mathbf{Y} = i\lambda\mathbf{Y} \quad (40)$$

where $\mathbf{Y} = (p, -P^*, q, -Q^*, r, -R^*)^T$ and \mathbf{A} is the (6×6) matrix:

$$\mathbf{A} = \begin{pmatrix} a_{11} & -a^2(\rho_r - i\rho_{im}) & -\epsilon & 0 & 0 & 0 \\ (a^*)^2(\rho_r + i\rho_{im}) & a_{22} & 0 & \epsilon & 0 & 0 \\ -\epsilon & 0 & E - 2|b|^2 & b^2 & -\epsilon & 0 \\ 0 & \epsilon & -(b^*)^2 & -E + 2|b|^2 & 0 & \epsilon \\ 0 & 0 & -\epsilon & 0 & a_{55} & -c^2(\rho_r + i\rho_{im}) \\ 0 & 0 & 0 & \epsilon & (c^*)^2(\rho_r - i\rho_{im}) & a_{66} \end{pmatrix} \quad (41)$$

where

$$\begin{aligned} a_{11} &= E + i\gamma + 2|a|^2(\rho_r - i\rho_{im}) \\ a_{22} &= -E + i\gamma - 2|a|^2(\rho_r + i\rho_{im}) \\ a_{55} &= E - i\gamma + 2|c|^2(\rho_r + i\rho_{im}), \\ a_{66} &= -E - i\gamma - 2|c|^2(\rho_r - i\rho_{im}). \end{aligned} \quad (42)$$

The solution of this 6×6 eigenvalue problem (and whether the corresponding eigenvalues λ possess a positive real part) will determine the spectral stability properties of the solutions of the nonlinear-PT-symmetric trimer.

C. Numerical Results for the Trimer Case

• Trimer Case I:

The numerical results for the symmetric solutions of the nonlinear-PT-symmetric trimer (Case I) are shown in Fig. 4, Fig. 5 and Fig. 6, with similar notations as in the dimer case. Solutions are found by numerically solving Eq. (34). A typical example of the branches that may arise in case I of the trimer is shown for the parameters $\epsilon = 1$, $E = 1$, $\rho_r = -1$ and $\rho_{im} = 1$. In this case, we find three branches in the considered interval of parameter values. There are two branches which exist up to the point $\gamma = 2.59$ where they collide in a saddle-node bifurcation. One of these, the red diamonds branch, is mostly unstable except for $\gamma \in [1.26, 1.33] \cup [2, 2.11]$. For $\gamma < 1.26$, this branch has one real and one imaginary pair, which become both imaginary for $\gamma > 1.26$ until they collide for $\gamma = 1.33$ and yield a complex quartet, which subsequently splits into two imaginary pairs for $\gamma = 2$ and finally into one real and one imaginary pair for $\gamma > 2.11$. The other one, the black squares branch, is always unstable due to one real and one imaginary pair. When these two modes collide, a collision arises between both their real and their imaginary (respective) eigenvalue pairs.

Aside from the other two branches, the branch associated with the blue stars emerges from $\gamma = 1$ and persists beyond the above critical point (and for all values of γ that we have monitored). In our case, this branch is only stable for $\gamma < 1.25$, at which two pairs of imaginary eigenvalues collide and lead to a complex quartet, which renders the branch unstable thereafter. This branch behaves very similarly as the one in the linear PT trimer case reported in [13]. Both of them bifurcate from zero amplitude after a certain value of γ , persist beyond the linear PT critical point and have similar stability properties.

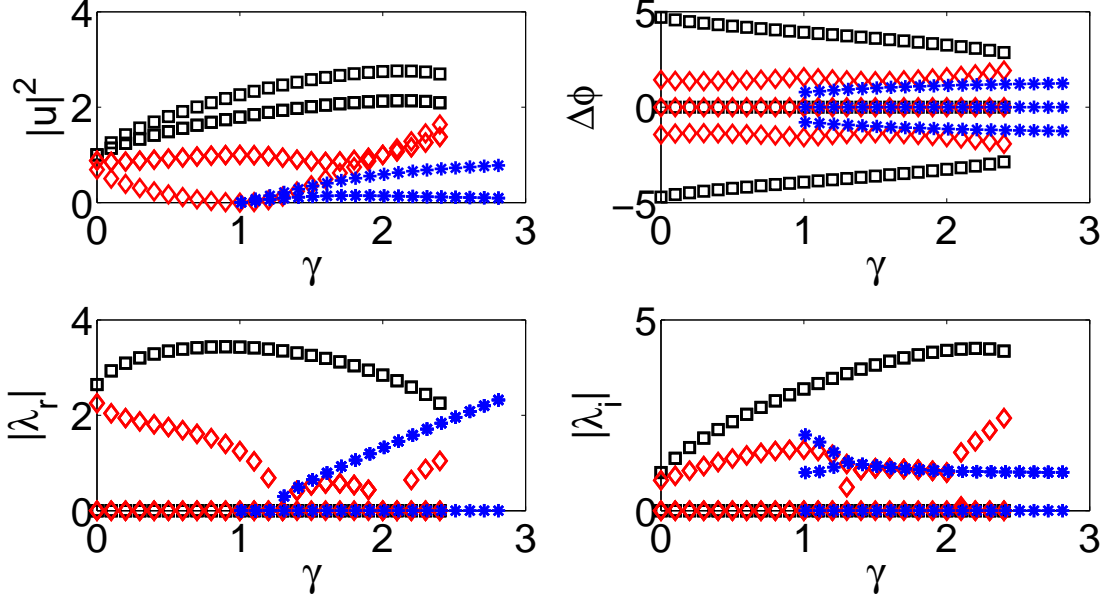


FIG. 4: The symmetric solution profiles of Case I in the nonlinear-PT-symmetric trimer with $\epsilon = 1$, $E = 1$, $\rho_r = -1$ and $\rho_{im} = 1$. The three branches are denoted by blue stars, red diamonds and black squares and their amplitudes (top left), phases (top right), real part (bottom left) and imaginary part (bottom right) of the corresponding eigenvalues are shown. See also the relevant discussion in the text.

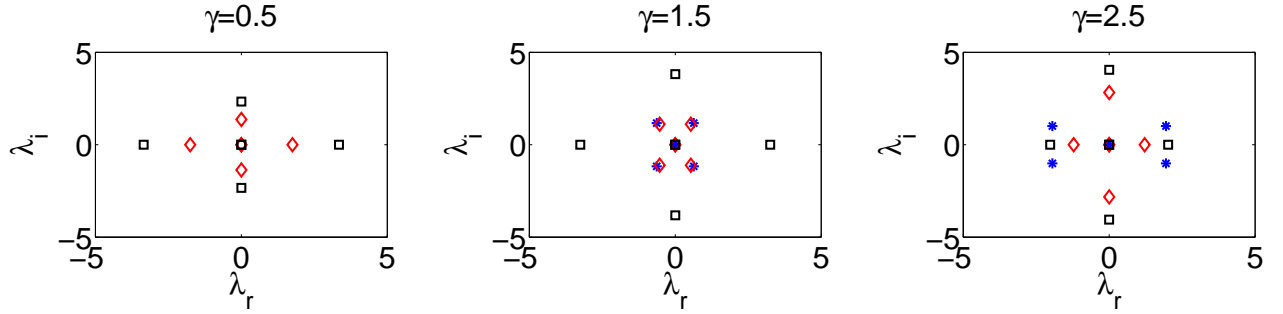


FIG. 5: The spectral plane of the linear stability analysis for the symmetric solutions of Case I with $\epsilon = 1$, $E = 1$, $\rho_r = -1$ and $\rho_{im} = 1$, for three different values of $\gamma = 0.5$, 1.5 and 2.5 . Each branch is associated with three eigenvalue pairs one of which is at 0 due to symmetry.

To monitor the dynamical evolution of the different branches, we used direct numerical simulations illustrated in Fig. 6 for the case of $\gamma = 1.5$. Two of the branches, the blue stars of the left panel and the red diamonds of the middle one are oscillatorily unstable for this value of γ , while the black squares branch is always unstable due to a real eigenvalue pair. The latter has been found to generically cause the unbounded gain of at least one node within the trimer. The oscillatory instability, on the other hand, in the case of the blue branch and for $\gamma = 1.5$ can be observed to lead to a long-lived periodic exchange of “power” between the three sites. On the other hand, for the red diamonds branch of the middle panel, while there is an intermediate stage of power oscillations between the three nodes, the ultimate fate of the configuration favors the unbounded growth of at

least one node (in fact, two nodes in the example shown) of the trimer.

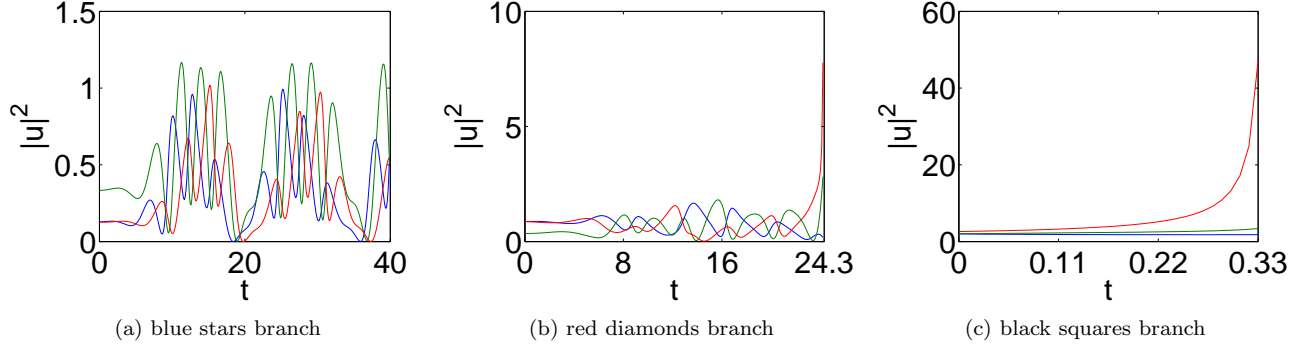


FIG. 6: The time evolution plots of the trimer case I with $\epsilon = 1$, $E = 1$, $\rho_r = -1$ and $\rho_{im} = 1$ when $\gamma = 1.5$. For each branch, the blue line denotes the nonlinear loss/linear gain site, the red line denotes the nonlinear gain/linear loss site, while the green represents the inert site between the two. Notice the oscillatory evolution of the blue solid branch, while the red diamonds and black squares lead to ultimate unbounded increase of at least one site within the trimer.

• Trimer Case II:

According to Eq. (35), one of the parameters should be determined by the others. We hereby set $\epsilon = 1$, $\rho_r = -1$ and $\rho_{im} = 1$, then E is obtained self-consistently for a given choice of γ . The solution profiles, which are obtained by solving Eq. (35) numerically, are plotted in Fig. 7. There are three pairs of branches, i.e., six branches of solutions in total found in this case. Only one out of each pair is shown in Fig. 7-9 (to avoid cluttering of the relevant figures), namely the blue stars, red diamonds and black squares. The other three branches are mirror symmetric to these branches, respectively. For example, the existence profile of the mirror symmetric branch of the blue stars would be identical to the blue stars shown in Fig. 7, while its stability plot would be mirror symmetric about the imaginary axis to the blue stars shown in Fig. 8. Among the three branches shown in Fig. 7, two of them emerge at $\gamma = 2$ and persist throughout the range of γ values considered. It should be noticed that the amplitudes are different within each branch. The blue stars (dynamically stable) branch has a large A and small B and C , while the red diamonds and black squares branches have a fairly small A and large values of B and C . In fact, precisely at the critical point of the branches' emergence, the blue stars and the black squares are exact mirror images of each other (i.e., they have the same amplitude for B and the one's A is the other's C -and vice versa-). This mirror symmetry is in fact directly reflected in the eigenvalues of the linearization around the two configurations, one set of which (for the blue stars) possesses negative real parts, while the other (black squares) has mirror symmetric positive ones. As can be perhaps intuitively anticipated, the more stable configuration is the one having large amplitude at the nonlinear loss/linear gain site. The third branch (red diamonds) is also highly unstable and emerges out of a bifurcation at $\gamma = 2.05$ (to which we will return when discussing case III).

Fig. 8 shows the eigenvalues of the three branches clearly illustrating the fact that they are not symmetric about the imaginary axis. This can once again be justified by the asymmetry of the configurations of case II which, in turn, break the PT symmetry of the linearization matrix and hence lead to asymmetric spectra. The blue stars branch is always stable, as indicated above, and the other two branches are always unstable as γ increases. For instance, for the red diamond branch, there exists (in addition to a zero eigenvalue) an imaginary pair, a complex conjugate pair (with a positive real part) and a real eigenvalue. In the case of the black squares branch, there are (in addition to the zero eigenvalue) three real pairs (two positive and one negative) and a complex conjugate pair (with positive real part).

Fig. 9 shows the dynamical plots of the three distinct branches of solutions. The blue stars branch clearly preserves its configuration due to its dynamical stability, while for the two unstable branches, their evolution gives rise to asymmetric dynamics favoring the loss of the power in a single site (the nonlinear gain/linear loss one), and quickly absorbed by a stable state. The latter state appears to be the mirror symmetric of the red diamonds asymmetric branch in both cases. This is indeed also a stable dynamical state of the original stationary system of equations. Furthermore, this state is expected to exist based on the symmetry breaking bifurcation that we will discuss below as giving rise to the red diamonds branch. As remarked above, the stability properties of the mirror symmetric branches are mirror symmetric to the ones shown in Fig. 8. This implies that only the mirror symmetric branch of the red diamonds is stable, which is, in turn, consonant with our observation that it is a potential attractor for the dynamics for $\gamma = 3$ shown in Fig. 9.

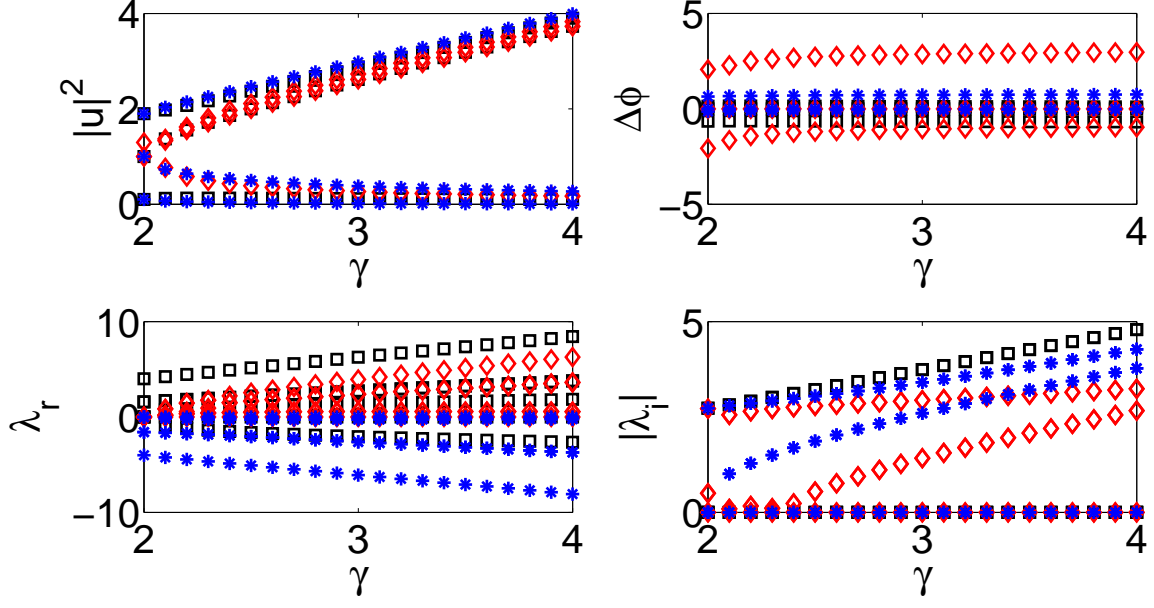


FIG. 7: The solution profile of the trimer case II with $\epsilon = 1$, $\rho_r = -1$ and $\rho_{im} = 1$. The three branches are denoted by blue stars, red diamonds and black squares. These branches start at $\gamma = 2$ (except for the red diamonds branch that is initiated at $\gamma = 2.05$) and exist even when γ is large.

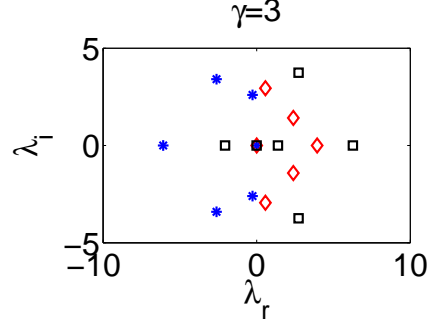


FIG. 8: The spectral stability plots of the trimer case II with $\epsilon = 1$, $\rho_r = -1$ and $\rho_{im} = 1$, illustrating the stability of the blue stars' branch and the instability of the other two.

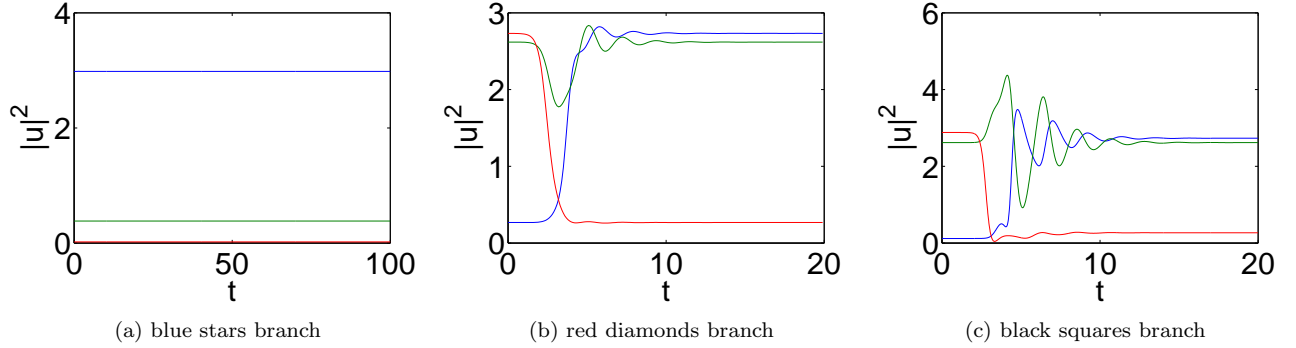


FIG. 9: The time evolution plots of the trimer case II with $\epsilon = 1$, $\rho_r = -1$ and $\rho_{im} = 1$ when $\gamma = 3$. The two unstable branches (red diamonds and black squares) tend to a dynamically stable configuration which is a mirror image of the red diamonds branch.

- Trimer Case III:

Finally, we turn to a consideration, using the same parametric setting as in case II, of the numerical results by solving Eq. (38) for case III in Figs. 10-12. Four distinct branches of solutions are observed in this case. The branches denoted by red diamonds and black squares exist only for small values of the linear gain/loss parameter γ , are stable and terminate at $\gamma = 0.65$. The other two branches, namely the blue stars and the green circles collide and terminate at $\gamma = 2.1$. The green circles branch is unstable in this case, due to a complex quartet of eigenvalues (observed in Fig. 11). On the other hand, the blue stars' branch is stable up to $\gamma = 2.05$ a critical point at which branches of case II (the red diamonds branch referred to in case II as having a pitchfork bifurcation at the same value and its mirror symmetric image) emerge. Notice that this detail is not discernible in the eigenvalue plots of Fig. 10.

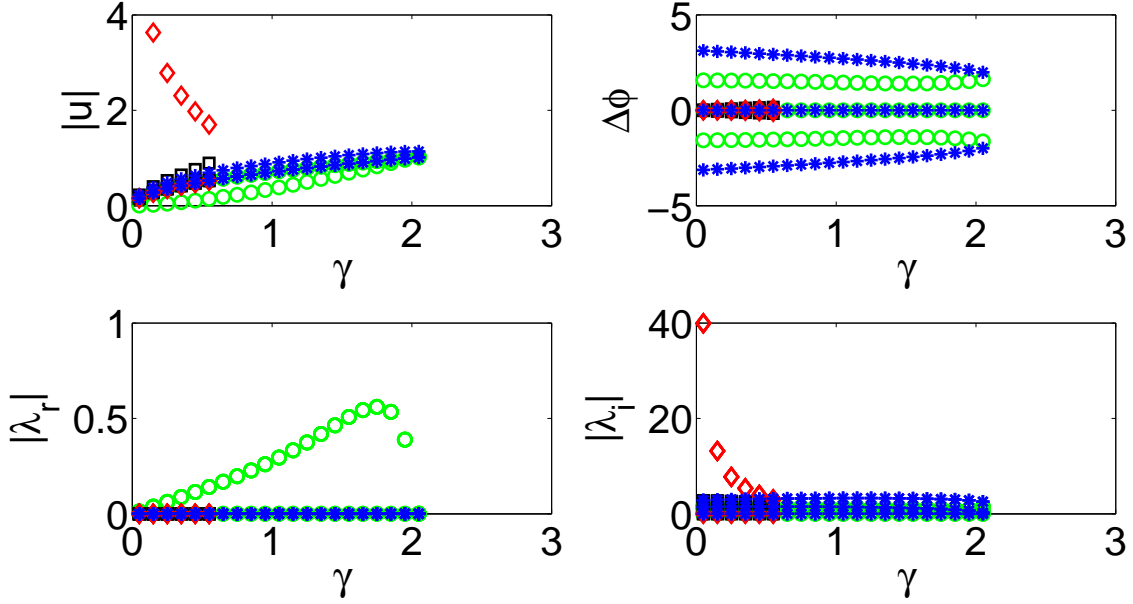


FIG. 10: The solution profile for the nonlinear-PT-symmetric trimer of Case III (special symmetric solutions) with $\epsilon = 1$, $\rho_r = -1$ and $\rho_{im} = 1$. The norms are not squared in the top left panel to improve the visibility of the branches (given the disparity of the relevant amplitudes). The four branches are denoted by blue stars, red diamonds, black squares and green circles. The blue stars, red diamonds and black squares branches always have two pairs of purely imaginary eigenvalues, while the green circles branch always has a complex quartet. The blue stars branch terminates with the green circles at $\gamma = 2.1$, while the red diamonds and black squares terminate together at $\gamma = 0.65$.

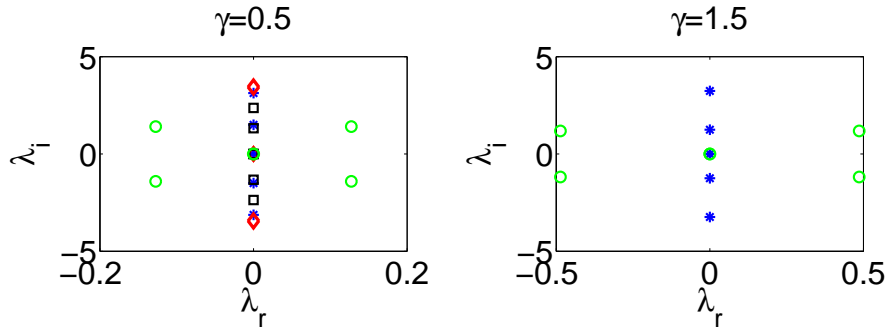


FIG. 11: The plots of the spectral plane of the linear stability eigenvalues for the nonlinear-PT-symmetric trimer Case III (special symmetric solutions) with $\epsilon = 1$, $\rho_r = -1$ and $\rho_{im} = 1$.

The dynamics of the different configurations are shown in Fig. 12. The blue stars, red diamonds and black squares special symmetric branches of solutions are stable and thus preserve their shape. On the other hand,

the green circles for $\gamma = 0.5$ are subject to the oscillatory instability predicted by the linear stability analysis. This, in turn, results into long-lived oscillatory dynamics of the system, as indicated in the bottom right of Fig. 12.

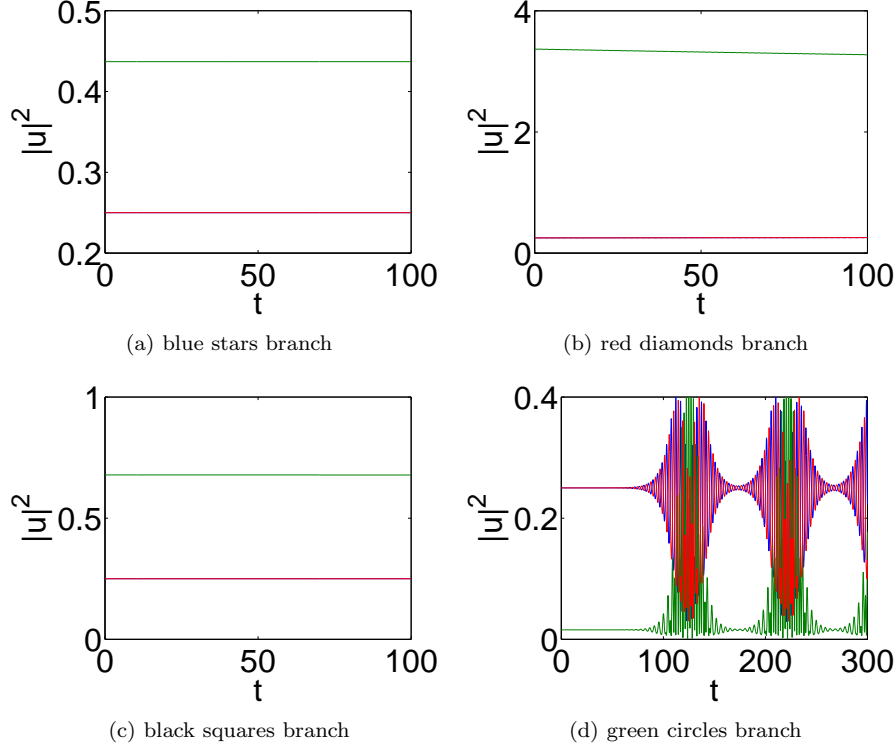


FIG. 12: The time evolution plots of the nonlinear-PT-symmetric trimer in Case III of special symmetric solutions with $\epsilon = 1$, $\rho_r = -1$ and $\rho_{im} = 1$ when $\gamma = 0.5$. The only unstable configuration is the green circle one of the bottom right which leads to long-lived oscillatory dynamics.

IV. THE SPECIAL CASE OF LINEAR-PT-SYMMETRIC OLIGOMERS

As a special case with $\rho_r = -1$ and $\rho_{im} = 0$ of what we did above, the linear PT-symmetric oligomer case example has been addressed in the earlier work of [13].

Fig. 13 shows the profile of the two branches, which are analogues of the nonlinear-PT-symmetric dimer displayed in Fig. 1. The branch denoted by dashed line corresponds to the blue stars branch of case I within the nonlinear-PT-symmetric dimer with $(-)$ sign in Eq. (11) and is stable when $\gamma^2 \leq k^2 - E^2/4$, whereas the solid line branch corresponding to the red diamonds branch (of case I in the nonlinear-PT-symmetric dimer) is always stable. The linearization around these branches can be performed explicitly in this simpler linear-PT-symmetric case yielding the nonzero eigenvalue pairs $\pm 2i\sqrt{2(\epsilon^2 - \gamma^2) - E\sqrt{\epsilon^2 - \gamma^2}}$ for the first and $\pm 2i\sqrt{2(\epsilon^2 - \gamma^2) + E\sqrt{\epsilon^2 - \gamma^2}}$ for the second (notice that the latter can never become real).

It is relevant to note here that the two branches “die” in a saddle-center bifurcation at $\gamma = \epsilon$, as shown in the figure. This point coincides with the linear PT-symmetric dimer phase transition. As indicated before, in the nonlinear dimer, the two branches die when the restriction (12) is no longer satisfied. Nevertheless, the nonlinear solutions of the latter case can generally exist past the linear phase transition (and even arbitrarily past that as in the case II solutions) and moreover asymmetric solutions can exist due to the interplay of linear and nonlinear gain/loss a feature absent in the simpler linear-PT-symmetric dimer.

As an analogue of the case I solutions of the nonlinear-PT-symmetric trimer, we present a prototypical example of the branches that may arise in the case of the linear-PT-symmetric trimer in Fig. 14 for $E = \epsilon = 1$. There are three distinct branches. Two of them collide in a saddle-center bifurcation (for $\gamma = 1.043$) and disappear thereafter. The other one emerges and bifurcates from zero amplitude for $\gamma > \sqrt{2\epsilon^2 - E^2}$ and persists beyond the critical point of the linear PT phase transition $\gamma_{PT} = \sqrt{2}\epsilon$, (although it is unstable in that regime). Hence the feature of solutions

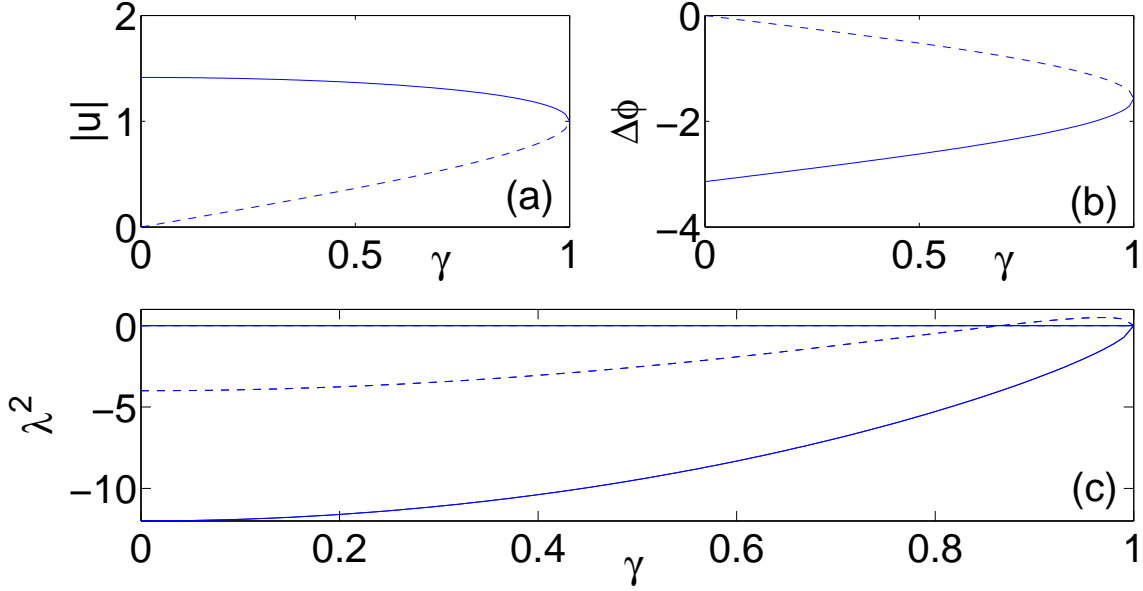


FIG. 13: (Color online) The two branches of solutions for the dimer problem are shown for parameter values $\epsilon = E = 1$. (a) The amplitude of the sites, (b) their relative phase, and (c) the (nontrivial) squared eigenvalue of the two branches. The solid line corresponds to the always stable branch, while the dashed line corresponds to the branch, which acquires a real eigenvalue pair above a certain $\gamma = \sqrt{\epsilon^2 - E^2/4}$. Reprinted with permission from [13].

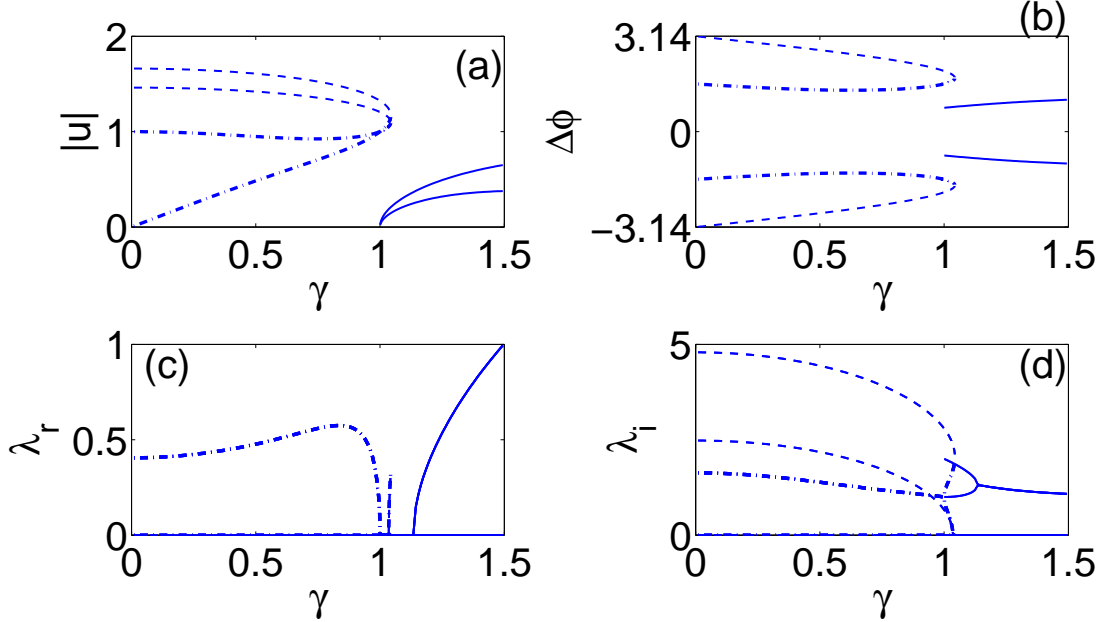


FIG. 14: (Color online) Existence and stability of solutions for the case of the trimer analogous to Fig. 13 with parameters $E = 1$ and ϕ_b normalized to 0 (without loss of generality). There are three branches: $u^{(1)}$ (dash-dotted line), $u^{(2)}$ (dashed line), and $u^{(3)}$ (solid line). For each branch, two curves in (a) stand for A, B, C (since $C = A$), and two curves in (b) stand for ϕ_a and ϕ_c . Panels (c) and (d) are the illustration of both real and imaginary parts for the eigenvalues. There exist two solutions (the dashed and the dash-dotted) one of which is stable (dashed) and one generically unstable (dash-dotted) which collide and disappear for $\gamma = 1.043$. The third solid branch emerges from the limit $\gamma = 1$ and persists thereafter (for all values of γ considered), although it becomes unstable for $\gamma > 1.13$. Reprinted with permission from [13].

persisting past the linear PT phase transition exists even in the linear-PT-symmetric trimer, yet other more complex features do not appear in this setting. A canonical example thereof is the existence of asymmetric solutions (which, in turn, possess asymmetric spectra). The latter trait is amply present in the nonlinear-PT-symmetric trimer of the previous section.

It should be added that in addition to the oligomers of the dimer and the trimer variety, recently there has also been considerable interest towards the study of quadrimer settings. Such settings were again initiated in the examination of [13], where the particular (and simpler) case of $(-i\gamma, -i\gamma, +i\gamma, +i\gamma)$ i.e., a linear-PT-symmetric quadrimer with two lossy sites on the one side and two gain nodes on the other side was considered. The considerations of [13] were generalized in the very recent study of [26], which examined the configuration $(-i\gamma_1, -i\gamma_2, +i\gamma_2, +i\gamma_1)$ i.e., the most general bi-parametric gain/loss family of quadrimers. In both cases, the possibility of solutions that emerge purely in the nonlinear regime and of ones that continue past the critical point of the underlying linear PT phase transition was identified. Another reason why such quadrimers are of interest is that they can be thought of as the prototypical building blocks (if placed on a square “plaquette”) of a two-dimensional PT-symmetric lattice [30]. To the best of our knowledge, nonlinear-PT-symmetric quadrimers, along the lines considered herein have not been examined to date.

V. CONCLUSIONS AND FUTURE CHALLENGES

In the above study, we illustrated some interesting characteristics which emanate from the interplay of nonlinearity with PT-symmetric linear Hamiltonians in the case of oligomer configurations. The basic underlying premise which has been explained in the recent works of [27, 30] and has been explored in numerous others such as [13, 24, 27, 30] is that the nonlinear and the PT-symmetric-linear part of the system at hand no longer commute and hence give rise to novel phenomenology that is not expected for linear PT symmetric systems. A principal element of this phenomenology that arises even for PT-symmetric oligomers (trimers, quadrimers, etc.) with merely linear gain/loss is the fact that nonlinear solutions may exist that do not have a corresponding linear limit and which, in fact, defy the threshold for the linear PT phase transition in that they exist for arbitrary gain/loss parameter values past that critical point. The introduction of a nonlinear gain/loss pattern considered herein for dimers and trimers (and earlier in a more cursory way in [24] for dimers) presents additional possibilities stemming from the interplay of linear and nonlinear gain/loss profiles. These include among others the emergence of asymmetric solutions which not only are involved in symmetry breaking (pitchfork) bifurcations but also produce asymmetric linearization matrices with spectral properties that reflect this asymmetry.

We believe that this direction of studies is particularly intriguing for further progress, especially as the complexity of the problem increases within the confines of a full one-dimensional chain, but also even for fundamental two-dimensional entities, such as the quadrimer based plaquettes. These themes constitute pristine territory for further exploration at the theoretical level. Naturally, on the other hand, a potential generalization of the earlier experiments of [5] towards the inclusion of nonlinear amplification and amplitude-dependent loss in balance with each other would be most worthwhile to consider in order to take advantage of the considerable additional wealth of phenomenology of the latter system.

Acknowledgments

PGK gratefully acknowledges support from the US National Science Foundation (grant DMS-0806762), the Alexander von Humboldt Foundation and the Alexander S. Onassis Public Benefit Foundation.

-
- [1] C.M. Bender and S. Boettcher, Phys. Rev. Lett. **80**, 5243 (1998); C.M. Bender, S. Boettcher and P.N. Meisinger, J. Math. Phys. **40**, 2201 (1999).
 - [2] Z.H. Musslimani, K.G. Makris, R. El-Ganainy and D.N. Christodoulides, Phys. Rev. Lett. **100**, 030402 (2008); K.G. Makris, R. El-Ganainy, D.N. Christodoulides and Z.H. Musslimani, Phys. Rev. A **81**, 063807 (2010).
 - [3] V. Achilleos, P.G. Kevrekidis, D.J. Frantzeskakis, R. Carretero-González, arXiv:1202.1310.
 - [4] A. Guo, G. J. Salamo, D. Duchesne, R. Morandotti, M. Volatier-Ravat, V. Aimez, G. A. Siviloglou and D. N. Christodoulides, Phys. Rev. Lett. **103**, 093902 (2009).
 - [5] C.E. Rüter, K.G. Makris, R. El-Ganainy, D.N. Christodoulides, M. Segev, D. Kip, Nature Phys. **6**, 192 (2010).
 - [6] J. Schindler, A. Li, M.C. Zheng, F.M. Ellis and T. Kottos, Phys. Rev. A **84**, 040101 (2011).
 - [7] H. Ramezani, T. Kottos, R. El-Ganainy and D.N. Christodoulides, Phys. Rev. A **82**, 043803 (2010).
 - [8] A.A. Sukhorukov, Z. Xu and Yu.S. Kivshar, Phys. Rev. A **82**, 043818 (2010).

- [9] M.C. Zheng, D.N. Christodoulides, R. Fleischmann and T. Kottos, Phys. Rev. A **82**, 010103(R) (2010).
- [10] E.M. Graefe, H.J. Korsch and A.E. Niederle, Phys. Rev. Lett. **101**, 150408 (2008).
- [11] E.M. Graefe, H.J. Korsch and A.E. Niederle, Phys. Rev. A **82**, 013629 (2010).
- [12] Z. Lin, H. Ramezani, T. Eichelkraut, T. Kottos, H. Cao and D.N. Christodoulides, Phys. Rev. Lett. **106**, 213901 (2011).
- [13] K. Li and P. G. Kevrekidis Phys. Rev. E **83**, 066608 (2011)
- [14] S.V. Dmitriev, S.V. Suchkov, A.A. Sukhorukov, and Yu.S. Kivshar, Phys. Rev. A **84**, 013833 (2011)
- [15] S.V. Suchkov, B.A. Malomed, S.V. Dmitriev and Yu.S. Kivshar, Phys. Rev. E **84**, 046609 (2011).
- [16] R. Driben and B. A. Malomed, Opt. Lett. **36**, 4323 (2011).
- [17] R. Driben and B. A. Malomed, Europhys. Lett. **96**, 51001 (2011).
- [18] F. Kh. Abdullaev, V.V. Konotop, M. Ögren and M. P. Sørensen, Opt. Lett. **36**, 4566 (2011).
- [19] N.V. Alexeeva, I.V. Barashenkov, A.A. Sukhorukov, and Yu.S. Kivshar, Phys. Rev. A **85**, 063837 (2012).
- [20] A.A. Sukhorukov, S.V. Dmitriev and Yu.S. Kivshar, Opt. Lett. **37**, 2148 (2012).
- [21] H. Cartarius and G. Wunner, Phys. Rev. A **86**, 013612 (2012); see also arXiv:1207.1669, J. Phys. A, in press (2012).
- [22] E.-M. Graefe, arXiv:1206.4806.
- [23] A.S. Rodrigues, K. Li, V. Achilleos, P.G. Kevrekidis, D.J. Frantzeskakis, C.M. Bender, arXiv:1207.1066.
- [24] A.E. Miroshnichenko, B.A. Malomed, and Yu.S. Kivshar Phys. Rev. A **84**, 012123 (2011).
- [25] F.Kh. Abdullaev, Y.V. Kartashov, V.V. Konotop and D.A. Zezyulin, Phys. Rev. A **83**, 041805 (2011)
- [26] D. A. Zezyulin, Y. V. Kartashov, V. V. Konotop, Europhys. Lett. **96**, 64003 (2011).
- [27] D. A. Zezyulin, V. V. Konotop, Phys. Rev. Lett. **108**, 213906 (2012).
- [28] M. Johansson, J. Phys. A: Math. Gen. **37**, 2201 (2004); R.H. Goodman, J. Phys. A: Math. Theor. **44**, 425101 (2011).
- [29] T. Kapitula, P. Kevrekidis, and Z. Chen, SIAM J. Appl. Dyn. Sys. **5**, 598 (2006).
- [30] K. Li, P.G. Kevrekidis, B.A. Malomed and U. Günther, Nonlinear PT-symmetric plaquettes, arXiv:1204.5530, J. Phys. A, in press (2012).